CrystEngComm

COMMUNICATION

View Article Online
View Journal | View Issue

Cite this: *CrystEngComm*, 2026, **28**, 2542

Received 6th February 2026,
Accepted 8th April 2026

DOI: 10.1039/d6ce00118a

rsc.li/crystengcomm

Single crystal growth and structural characterization of synthetic U(VI) peroxide phases, studtite ($UO_2(O_2)(H_2O)_2{\cdot}2H_2O$) and metastudtite ($UO_2(O_2)(H_2O)_2$)

Grant C. Benthin, Cameron J. Flester and Tori Z. Forbes *

A H_2O_2 vapor diffusion method resulted in the successful synthesis of uranyl peroxide, $UO_2(O_2)(H_2O)_2{\cdot}2H_2O$ (studtite) crystals, enabling the first direct structural refinement of synthetic material. Subsequent controlled dehydration of these crystals produced crystalline metastudtite, $UO_2(O_2)(H_2O)_2$, allowing for the experimental determination of its atomic structure.

Uranyl(VI) peroxide phases, studtite ($UO_2(O_2)(H_2O)_2{\cdot}2H_2O$) and its dehydrated analogue, metastudtite ($UO_2(O_2)(H_2O)_2$), play a significant role in the behavior of uranium in high radiation fields, such as those encountered during the corrosion of spent nuclear fuel (SNF).[1–3] These two phases are the only naturally occurring peroxide bearing mineral phases and have previously been identified within the oxidation rind of uraninite (UO_2) ore bodies.[4–6] Formation of the uranyl peroxide minerals likely occurs *via* alpha irradiation of surface-adsorbed water, which could produce H_2O_2 concentrations as high as 3.5×10^{-3} M.[7,8] The higher radiation field associated with the SNF enables water radiolysis to occur much more readily and studtite has previously been observed within laboratory-based corrosion studies[1,2,9–11] and on the surface of fuel debris associated with the Chernobyl site.[12] Metastudtite forms from the direct dehydration of studtite and is the thermodynamically stable uranyl peroxide phase.[13] While less commonly encountered as an alteration phase on SNF, metastudtite may play a role in the long-term evolution of uranyl peroxide solids under repository-relevant conditions due to this thermodynamic favorability.

Despite the importance of studtite and metastudtite, structural characterization of these phases, particularly metastudtite, has been limited. Reports with proposed unit cell parameters associated with studtite and metastudtite date back to the mid-1940s,[14] but the crystal structure of studtite was originally determined from a natural mineral specimen by Burns and Hughes in 2003.[3] No synthetic methods capable of yielding studtite crystals suitable for single-crystal X-ray diffraction (SCXRD) have been reported in literature. Similarly, metastudtite has only been structurally characterized using powder X-ray diffraction (PXRD) techniques, leaving its precise atomic structure unresolved through experimental methods.[2,15,16] Significant computational efforts reported by Weck *et al.* in 2012, resulted in the proposal of a computationally derived structure of metastudtite and remains the only reported structural description of this phase.[17]

Herein, we report a synthetic route that enables the growth of single crystals of studtite *via* vapor diffusion of hydrogen peroxide into acidified uranyl nitrate solutions. These crystals were of sufficient quality for SCXRD analysis, allowing us to confirm and refine the structure of studtite. Furthermore, we demonstrate that controlled dehydration of these crystals at low humidity yields single crystals of metastudtite, enabling the first SCXRD-based determination of its structure.

Laboratory-based studtite has previously been synthesized by adding an excess of H_2O_2 directly to acidified (10^{-6} – 2 M HNO_3) solutions of uranyl nitrate, but this method results in polycrystalline (<10 μm) materials (SI, Fig. S1a).[2,7,14,18–24] Given that U(VI) is known to complex with peroxide anions even at concentrations as low as 10^{-4} M,[9] we sought to control the growth of studtite crystals by slowly introducing H_2O_2 to the solution through vapor diffusion at 20 °C, using solutions contained in nested vials as described by Sommer.[25] 1 mL of 25 mM uranyl nitrate in varying concentrations of nitric acid (0.1–2 M) were first placed in a 3.5 mL glass vial. This vial was then nested in a 20 mL glass scintillation vial containing 1.5 mL of 30% H_2O_2 and the container was sealed with a lid. Over time, studtite crystals formed on the bottom of the small glass vial and the rate of crystal formation was found to depend on the acid concentration (SI, Fig. S1b–d). Onset of crystallization for

Department of Chemistry, University of Iowa, Iowa City, IA 52242, USA.
E-mail: tori-forbes@uiowa.edu

studtite from solutions containing 0.5 M HNO_3 occurred at 4 days and was completed after approximately 2 weeks. In contrast, a small amount of crystalline product formed in the 2 M HNO_3 after 2 weeks, but complete crystallization took up to 2 months. As one may expect, there was also a correlation between the rate of crystallization and the size and crystal quality of the product, with slower rates of crystallization leading to larger, higher-quality crystals. Single crystals as large as 10 × 10 × 200 μm were able to be reproducibly grown from H_2O_2 vapor diffusion with uranyl nitrate in 2 M nitric acid (SI, Fig. S1d). Attempts to grow single crystals from solutions with nitric acid concentrations greater than 2 M were unsuccessful and no solid material precipitated even at long reaction times (>1 year).

It is assumed that the slow diffusion of H_2O_2 vapor, mediated by the low vapor pressure of hydrogen peroxide, allows for hydrogen peroxide to be introduced to the acid solution slowly enough to nucleate and grow high quality single crystals. Semi-quantitative analysis of 2 M nitric acid samples set up for peroxide vapor diffusion showed that the peroxide concentration in the samples remained below approximately 0.2 μM for at least 64 days (SI, Fig. S2). In addition to the slow introduction of H_2O_2, the overall peroxide concentration could also be impacted by autocatalytic decomposition, although this typically occurs in >8 M HNO_3.[22,26,27]

Structural characterization of the crystals formed from the H_2O_2 vapor diffusion method was performed by SCXRD, resulting in data with good agreement to natural studtite reported by Burns *et al.*[3] The unit cell parameters of the synthetic studtite crystals, refined in the monoclinic space group $C2/c$ with a = 13.999(1) Å, b = 6.7481(7) Å, c = 8.4848(9) Å, β = 123.143(3)° (SI, Table S1), are all within 1% of the previously reported values. Notably, the structure of synthetic studtite was analyzed at 100 K, whereas the structure reported by Burns *et al.*[3] was determined at 293 K. This difference in temperature may contribute to minor variations in refined structural parameters due to thermal contraction at lower temperature. The structure contains U(VI) with two strong bonds to oxygen atoms to create the nearly linear dioxo cation $(UO_2)^{2+}$. The U(VI) cation is further bound to six O atoms arranged at the equatorial vertices of a distorted hexagonal bipyramid, with two opposing vertices corresponding to aqua ligands and the other four vertices corresponding to two bidentate peroxide ligands (Fig. 1A). Adjacent uranyl moieties are linked through bridging μ_2-peroxide groups, creating 1-D chains that propagate parallel to the c-axis (Fig. 1C). The U–O_2–U dihedral angle within the chains is 126.3°, which is within 1% of the previously reported structure by Burns *et al.*[3] Within the interstitial regions between adjacent chains, there are also two additional water molecules that mediate interaction between nearby chains through a series of hydrogen bonds. Each interstitial water molecule accepts two hydrogen bonds from aqua ligands, with donor–acceptor (D···A) distances of 2.687(8) Å and 2.691(8) Å, and each donates a hydrogen bond to a uranyl oxo and a peroxide group on adjacent chains (D···A of 2.876(9) and 2.74(1) Å, respectively). Comparison of the bond lengths between the two structures reveals that all the U–O bond lengths (U=O_{yl}, U–O_{peroxo}-, and U–O_{aqua}) are within 1.2% of the previously reported values (SI, Table S2). The largest deviation in bond length between the synthetic and natural studtite is that of the O–O peroxide bond, which is shorter in the natural sample by 2.4%, from 1.50(1) to 1.46(1) Å. Recent results from Scherrer *et al.* could support the hypothesis that the O–O bond may be contracted due to the accumulation of superoxide ($O_2^{\bullet-}$) in place of the peroxide (O_2^{2-}) as a result of self-radiolysis of natural specimens, but

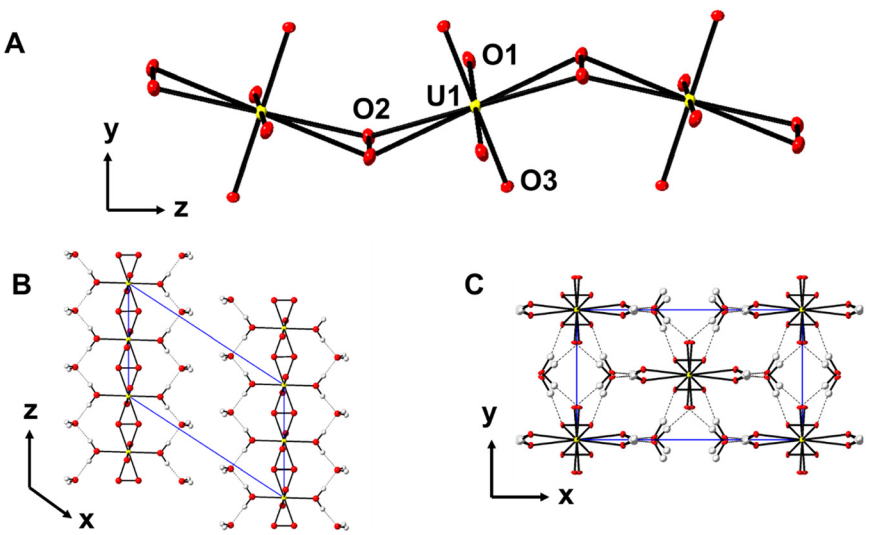

Fig. 1 (A) Structural characterization of synthetic studtite indicates the formation of one-dimensional uranyl peroxide chains. The U, O, and H atoms are represented by the yellow, red and white thermal ellipsoids, respectively. (B) Each chain is further engaged in hydrogen bonding (indicated by the dashed line) between the ligated and interstitial water molecules. (C) The three-dimensional lattice is formed through additional hydrogen bonding interactions between the interstitial water and the uranyl oxo and peroxide ligands.

additional EPR spectroscopy would be necessary to provide confirmation.[28]

With the ability to reliably grow single crystals of studtite, we sought to elucidate the crystal structure of metastudtite by dehydrating synthetic material. Heating studtite crystals to 80 °C for 18 h resulted in dehydration, but also degraded the crystallinity of the material, such that it was functionally impossible to manipulate single crystals to collect structural data. Although dehydration at elevated temperatures (50–100 °C) is the most reported synthetic strategy for dehydrating studtite to metastudtite,[10,15,23,29–31] reports by Huttig *et al.* and Li *et al.* suggest exposure to a low humidity environment could also cause dehydration of solid-state material.[32,33] Therefore, a 400 mg sample of the crystalline studtite was placed into a sealed jar containing calcium sulfate desiccant to create a low relative humidity (<5%) environment for dehydration. After one week, the reacted material was evaluated using PXRD (SI, Fig. S3) and Raman spectroscopy (SI, Fig. S4 and S5), and this analysis confirmed that the initial studtite converted to metastudtite after exposure to these conditions. For structural characterization of metastudtite, single crystals of studtite were isolated, dehydrated, and analyzed according to the procedure outlined in SI, section S3. Analysis of the studtite crystals exposed to the low relative humidity environment resulted in a change in the unit cell parameters from the monoclinic setting to the orthorhombic space group *Immm* where a = 4.1946(5) Å, b = 6.5143(9) Å, and c = 8.733(1) Å (see SI, Tables S1 and S3 for crystallographic details).

Further structural refinement of the metastudtite diffraction data indicates the presence of disordered one-dimensional chains of repeating $[UO_2(O_2)_2(H_2O)_2]$ subunits, linked through bridging peroxide ligands (Fig. 2). Disorder of the one-dimensional chains can be accounted for by the presence of mirror planes within the *Immm* space group, but modeling the structure in a lower symmetry space group or with a supercell did not resolve the issue (see SI, section S3.2 for additional details regarding these evaluations). Disorder can be resolved by separating the overlayed canting direction of the uranyl peroxide chains (Fig. 2A), which results in structural parameters that resemble that of the studtite. The crystallographically unique $(UO_2)^{2+}$ moiety contains U═O bond lengths of 1.80(2) Å and a linear (180°) O═U═O bond. Six equatorially-bound O atoms represented by two unique positions, O2 and O3, corresponding to *trans*-peroxo and aqua ligands, respectively. U–O2 and U–O3 bond lengths are 2.35(1) and 2.42(2) Å, respectively, and the O2–O2 peroxide bond distance of 1.47(4) Å and U–O_2–U dihedral angle of 125.6° are within the expected range for bridging peroxide bonds in uranyl peroxide materials.[34,35]

Dehydration results in the removal of the interstitial water molecules, resulting in hydrogen bonding occurring directly between the aqua ligands and the axial oxo or bridging peroxo ligands of the adjacent uranyl peroxide chains with donor to acceptor distances of 2.92(2) Å and 2.75(2) Å (Fig. 2B and C). Although the formal oxidation state of uranium remains U(VI) through the dehydration, the removal of interstitial water and reorganization of the hydrogen-bonding network are expected to subtly influence the local uranium bonding environment. In particular, the shift to more direct hydrogen bonding interactions with uranyl oxo and peroxo ligands may modify the electron density distribution at these sites. This is consistent with the observed increase in the ν_1 uranyl stretching frequency and suggests a modest strengthening of the U═O bond despite minimal changes in the refined bond lengths. Due to the

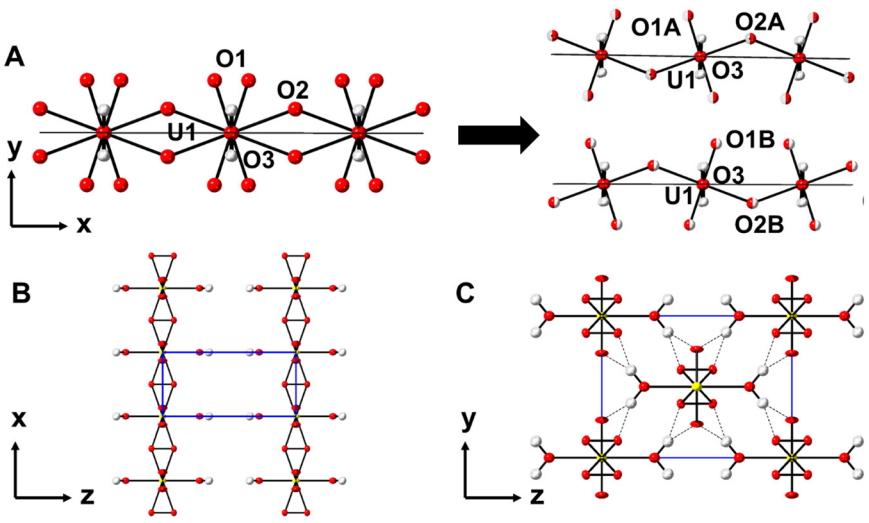

Fig. 2 (A) Structural characterization of synthetic metastudtite indicates the formation of disordered uranyl peroxide chains extending in the [100] direction. The disorder can be resolved by considering the superimposing two chains that are canted in opposite directions with O1 (A and B) and O2 (A and B) at half occupancy. The U, O, and H atoms are represented by the yellow, red and white spheres, respectively. (B) Absence of interstitial water molecules results in no hydrogen bonding interactions between the uranyl peroxide chains located in the same plane (020). (C) Hydrogen bonding between ligated water molecules and the uranyl oxo and peroxide ligands in neighboring chains is depicted as dashed lines.

disordered nature of the metastudtite structure, multiple configurations of adjacent uranyl peroxide chains exist within the structure. The two adjacent chains to a given aqua ligand can either be corrugated in sync or out of sync, giving rise to three possible hydrogen bonding conformations for each aqua ligand (SI, Fig. S7). Over the entire structure this results in the aqua ligands on average participating in three hydrogen bonding interactions with adjacent chains, two with oxo ligands and one with a peroxo ligand, regardless of the conformation of adjacent chains. This essential equivalence in the hydrogen bonding networks between chains provides a possible explanation for why the chains are disordered, as the hydrogen bonding networks would not be expected to appreciably stabilize or destabilize any specific chain conformation. This is different than what is observed for the studtite structure, where the interstitial water molecules provide additional hydrogen bonding that may guide the specifics of the uranyl chain configuration. The increase in hydrogen bonding contacts for the ligated water in metastudtite may also be a sound rationalization for increased thermodynamic stability and the irreversibility of the dehydration process.

Comparing our current results to previously reported structural information of metastudtite, indicates that the unit cell agrees well with previous values provided by PXRD[4,14,36] compared to the computational analysis by Weck *et al.*[17,37] Table 1 summarizes the structural parameters for metastudtite provided by SCXRD, PXRD, and computational analysis. The single-crystal and powder X-ray diffraction analysis both indicate an orthorhombic, *Immm*, space group with unit cell differences related to the specific cell setting. Differences to the computational data result from a doubling of one of the axes and lowering the orthorhombic setting from an I-centered to a primitive unit cell. These differences are also apparent in the calculated PXRD patterns from Weck *et al.*, with additional features at 21.1, 27.2, 29.4, 34.8, 39.9, 44.2, and 45.2° 2θ (Fig. 3). These features are absent in the calculated pattern from the SCXRD data as well as the PXRD pattern of the metastudtite solid synthesized herein. We also

Table 1 Structural parameters for metastudtite determined from SCXRD analysis, powder X-ray diffraction (PXRD) analysis by Debets,[14] and computational evaluation by Weck *et al.*[17]

Compound	Present work – SCXRD	Debets – PXRD	Weck *et al.* – computational
Structural formula	$(UO_2)O_2(H_2O)_2$	$UO_4{\cdot}2H_2O$	$(UO_2)O_2(H_2O)_2$
Formula weight (g)	338.06	338.06	338.06
Crystal system	Orthorhombic	Orthorhombic	Orthorhombic
a (Å)	4.1946(5)	6.50(2)	8.45
b (Å)	6.5143(9)	4.211(5)	8.72
c (Å)	8.733(1)	8.78(1)	6.75
α (°)	90	90	90
β (°)	90	90	90
γ (°)	90	90	90
Unit cell volume (Å^3)	238.65(6)	240(1)	497.4
Space group	*Immm*	*Immm*	*Pnma*
Z	2	2	4

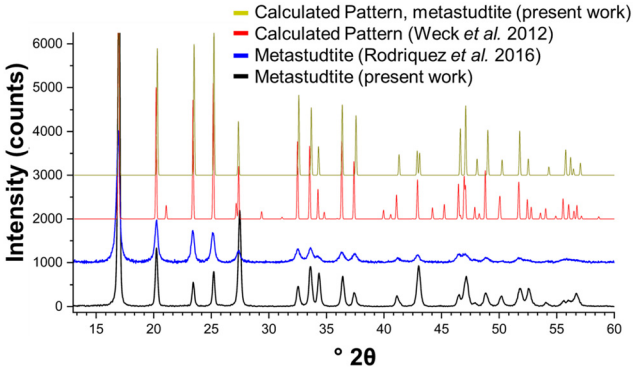

Fig. 3 Comparison of the PXRD patterns of metastudtite with calculated powder patterns based on the CIF files obtained by Weck *et al.*[17] and the present work. Identity of traces (from bottom to top): experimental PXRD pattern of metastudtite collected as a part of the present work (black), experimental PXRD pattern of metastudtite reported by Rodriguez *et al.*[37] (blue), calculated PXRD pattern based on metastudtite reported by Weck *et al.*[17] (red), and calculated PXRD pattern based on metastudtite reported in the present work (dark yellow).

more broadly evaluated previously reported metastudtite PXRD found in the literature, such as the data from Rodriguez *et al.*,[37] and found that it more closely matched the simulated pattern obtained from the SCXRD data.

The major differences between the theoretical (Weck *et al.*) and experimental (SCXRD) structures stem from ordering of adjacent uranyl peroxide chains rather than specific differences in bonding within the solid material. The DFT calculations accurately captured the one-dimensional chain structure and the U–O_2–U dihedral angle, but predicted that the cant direction would be ordered throughout the crystalline lattice. This ordering requires that the unit cell axis is doubled along the length of the chain to account for the two different orientations of the uranyl cation and peroxide anion. DFT calculation will provide the energy minimized structure, which likely is an ordered arrangement of the uranyl peroxide chains. However, experimentally, we arrive at metastudtite *via* a dehydration reaction, which may lead to disorder of the structure as the hydrogen bonding network is disrupted throughout the process. This reaction would not be captured in the theoretical study and even accurately calculating changes in hydrogen bonding networks is inherently challenging for DFT without special treatments such as van der Waals dispersion correction schemes and Hubbard U corrections.[38] This does potentially suggest that there could be restructuring of the metastudtite structure upon aging for it to reach the possible energy minimum structure that is predicted by Weck *et al.*, but further studies are necessary to confirm this hypothesis.

The current study provides a reliable method to grow single crystals of studtite through the vapor diffusion of hydrogen peroxide, representing an advancement in the synthetic chemistry of insoluble peroxide materials. This technique overcomes the longstanding limitations in the analysis of synthetic studtite samples with poor crystallinity,

which can then be successfully dehydrated to form metastudtite. Analysis of metastudtite with SCXRD, represents the first experimental structural characterization and revealed disorder in the 1-D chain that differs from previous computational results. Overall, these results not only expand experimental abilities for studying uranyl peroxide phases, but also expand our understanding of the structural transformations that occur during the formation of alteration phases of uranium-containing materials, with implications for nuclear waste management and repository science.

Author contributions

The research project was conceived by T. Z. F. and G. C. B. All single-crystal experiments and data analysis were performed by G. C. B. in consultation with T. Z. F. Powder dehydration experiments and the collection of all PXRD data was performed by C. J. F. G. C. B. and T. Z. F. wrote the manuscript. All authors contributed to discussions about the experimental results and final edits of the manuscript. Funding was secured by T. Z. F.

Conflicts of interest

The authors declare no competing interests.

Data availability

The data supporting this article have been included as part of the supplementary information (SI).

Supplementary information: synthetic details, PXRD data, Raman spectra, SCXRD details and data. See DOI: https://doi.org/10.1039/d6ce00118a.

CCDC 2528711 and 2528712 contain the supplementary crystallographic data for this paper.[39a,b]

Acknowledgements

G. C. B., C. J. F., and T. Z. F. acknowledge funding support for this work is provided by the U.S. Department of Energy, Basic Energy Sciences, Heavy Elements Chemistry program under DE-SC0023995. We gratefully acknowledge Dr. Daniel Unruh from the Materials Analysis, Testing, and Fabrication (MATFab) Facility at the University of Iowa for valuable guidance and support with crystallographic data analysis.

References

1 B. McNamara, E. Buck and B. Hanson, Observation of Studtite and Metastudtite on Spent Fuel, *Mater. Res. Soc. Symp. Proc.*, 2003, **757**, 401–406, DOI: 10.1557/PROC-757-II9.7.

2 B. D. Hanson, B. McNamara, E. C. Buck, J. I. Friese, E. Jenson, K. Krupka and B. W. Arey, Corrosion of commercial spent nuclear fuel. 1. Formation of studtite and metastudtite, *Radiochim. Acta*, 2005, **93**(3), 159–168, DOI: 10.1524/ract.93.3.159.61613, (acccessed 2025-09-05).

3 P. C. Burns and K.-A. Hughes, Studtite, [(UO2)(O2)(H2O)2](H2O)2: The first structure of a peroxide mineral, *Am. Mineral.*, 2003, **88**(7), 1165–1168, DOI: 10.2138/am-2003-0725, (acccessed 7/16/2024).

4 M. Deliens and P. Piret, Metastudtite, UO 4. 2H 2 O, a new mineral from Shinkolobwe, Shaba, Zaire, *Am. Mineral.*, 1983, **68**(3–4), 456–458.

5 J. F. Vaes, Six New Uranium Minerals from Shinkolobwe (Katanga), *Ann. Soc. Geol. Belg.*, 1946, **A-6B 70**, B212–B225.

6 J. Plasil, Oxidation-hydration weathering of uraninite: the current state-of-knowledge, *J. Geosci.*, 2014, **59**(2), 99–114.

7 K.-A. H. Kubatko, K. B. Helean, A. Navrotsky and P. C. Burns, Stability of Peroxide-Containing Uranyl Minerals, *Science*, 2003, **302**(5648), 1191–1193, DOI: 10.1126/science.1090259.

8 G. Sattonnay, C. Ardois, C. Corbel, J. F. Lucchini, M. F. Barthe, F. Garrido and D. Gosset, Alpha-radiolysis effects on UO2 alteration in water, *J. Nucl. Mater.*, 2001, **288**(1), 11–19, DOI: 10.1016/S0022-3115(00)00714-5.

9 F. Clarens, J. de Pablo, I. Díez-Pérez, I. Casas, J. Giménez and M. Rovira, Formation of Studtite during the Oxidative Dissolution of UO2 by Hydrogen Peroxide: A SFM Study, *Environ. Sci. Technol.*, 2004, **38**(24), 6656–6661, DOI: 10.1021/es0492891.

10 R. Kusaka, Y. Kumagai, T. Yomogida, M. Takano, M. Watanabe, T. Sasaki, D. Akiyama, N. Sato and A. Kirishima, Distribution of studtite and metastudtite generated on the surface of U3O8: application of Raman imaging technique to uranium compound, *J. Nucl. Sci. Technol.*, 2021, **58**(6), 629–634, DOI: 10.1080/00223131.2020.1854881.

11 A. Perrot, A. Canizares, S. Miro, L. Claparede, R. Podor, T. Sauvage, S. Peuget, C. Jegou and N. Dacheux, In situ Raman monitoring of studtite formation under alpha radiolysis in 18O-labeled water, *J. Nucl. Mater.*, 2024, **600**, 155267, DOI: 10.1016/j.jnucmat.2024.155267.

12 B. E. Burakov, E. E. Strykanova and E. B. Anderson, Secondary Uranium Minerals on the Surface of Chernobyl "Lava", *MRS Online Proc. Libr.*, 1996, **465**(1), 1309–1311, DOI: 10.1557/PROC-465-1309.

13 P. F. Weck and E. Kim, Uncloaking the Thermodynamics of the Studtite to Metastudtite Shear-Induced Transformation, *J. Phys. Chem. C*, 2016, **120**(30), 16553–16560, DOI: 10.1021/acs.jpcc.6b05967.

14 P. C. Debets, X-ray diffraction data on hydrated uranium peroxide, *J. Inorg. Nucl. Chem.*, 1963, **25**(6), 727–730, DOI: 10.1016/0022-1902(63)80165-7.

15 X. Guo, S. V. Ushakov, S. Labs, H. Curtius, D. Bosbach and A. Navrotsky, Energetics of metastudtite and implications for nuclear waste alteration, *Proc. Natl. Acad. Sci. U. S. A.*, 2014, **111**(50), 17737–17742, DOI: 10.1073/pnas.1421144111.

16 S. Bastians, G. Crump, W. P. Griffith and R. Withnall, Raspite and studtite: Raman spectra of two unique minerals, *J. Raman Spectrosc.*, 2004, **35**(8–9), 726–731, DOI: 10.1002/jrs.1176.

17 P. F. Weck, E. Kim, C. F. Jové-Colón and D. C. Sassani, Structures of uranyl peroxide hydrates: a first-principles

study of studtite and metastudtite, *Dalton Trans.*, 2012, **41**(32), 9748–9752, DOI: 10.1039/C2DT31242E.

18 F. Colmenero, L. J. Bonales, J. Cobos and V. Timón, Study of the thermal stability of studtite by in situ Raman spectroscopy and DFT calculations, *Spectrochim. Acta, Part A*, 2017, **174**, 245–253, DOI: 10.1016/j.saa.2016.11.040.

19 N. Hibert, B. Arab-Chapelet, M. Rivenet, L. Venault, C. Tamain and O. Tougait, Coprecipitation of actinide peroxide salts in the U–Th and U–Pu systems and their thermal decomposition, *Dalton Trans.*, 2022, **51**(34), 12928–12942, DOI: 10.1039/D2DT02376H.

20 T. Sato, Preparation of uranium peroxide hydrates, *J. Appl. Chem.*, 1963, **13**(8), 361–365, DOI: 10.1002/jctb.5010130807.

21 A. S. Kornilov, E. V. Piterkina, K. O. Shcherbakova, A. O. Makarov and O. S. Dmitrieva, Specific Features of Peroxide Precipitation of Uranium from Acid Water–Ethanol Solutions, *Radiochemistry*, 2020, **62**(2), 173–176, DOI: 10.1134/S1066362220020046.

22 L. Muller, P. Estevenon, C. Tamain, N. Dacheux and N. Clavier, Precipitation of morphology-controlled uranium(VI) peroxide in nitric acid media, *Dalton Trans.*, 2025, **54**(17), 6847–6857, DOI: 10.1039/D4DT03467H.

23 K.-W. Kim, K.-Y. Lee, Y.-J. Baek, D.-Y. Chung, E.-H. Lee and J.-K. Moon, Evaluation of the stability of precipitated uranyl peroxide and its storage characteristics in solution, *J. Nucl. Sci. Technol.*, 2016, **53**(2), 263–270, DOI: 10.1080/00223131.2015.1038662.

24 D. V. Kravchuk and R. E. Wilson, Reactions of Studtite UO4·4H2O in Alkali Hydroxides: Isolation of Single-Crystal Uranate Phases under Mild Hydrothermal Conditions, *Cryst. Growth Des.*, 2025, **25**(17), 7166–7173, DOI: 10.1021/acs.cgd.5c00701.

25 R. Sommer, How to grow crystals for X-ray crystallography, *Acta Crystallogr., Sect. C: Struct. Chem.*, 2024, **80**(8), 337–342, DOI: 10.1107/S2053229624006624.

26 D. Sicsic, F. Balbaud-Célérier and B. Tribollet, Mechanism of Nitric Acid Reduction and Kinetic Modelling, *Eur. J. Inorg. Chem.*, 2014, **2014**(36), 6174–6184, DOI: 10.1002/ejic.201402708.

27 R. E. Elson, *The Homogeneous Decomposition of Hydrogen Peroxide by Plutonium(IV)*, UCRL-6536, California Univ., Lawrence Radiation Lab., Livermore, United States, 1961, DOI: 10.2172/4834038.

28 S. K. Scherrer, C. Gates, H. Rajapaksha, S. M. Greer, B. W. Stein and T. Z. Forbes, Superoxide Radicals in Uranyl Peroxide Solids: Lasting Signatures Identified by Electron Paramagnetic Resonance Spectroscopy, *Angew. Chem., Int. Ed.*, 2024, **63**(21), e202400379, DOI: 10.1002/anie.202400379.

29 I. J. Schwerdt, A. Olsen, R. Lusk, S. Heffernan, M. Klosterman, B. Collins, S. Martinson, T. Kirkham and L. W. McDonald, Nuclear forensics investigation of morphological signatures in the thermal decomposition of uranyl peroxide, *Talanta*, 2018, **176**, 284–292, DOI: 10.1016/j.talanta.2017.08.020.

30 C. E. Chamberlain, T. L. Spano, R. D. Hunt, P. C. Burns and A. Miskowiec, Rehydration of metastudtite in the alteration kinetics of α– and β–U3O8 in dilute aqueous solutions of hydrogen peroxide, *J. Nucl. Mater.*, 2025, **615**, 155941, DOI: 10.1016/j.jnucmat.2025.155941.

31 T. L. Spano, J. L. Niedziela, A. E. Shields, J. McFarlane, A. Zirakparvar, Z. Brubaker, R. J. Kapsimalis and A. Miskowiec, Structural, Spectroscopic, and Kinetic Insight into the Heating Rate Dependence of Studtite and Metastudtite Dehydration, *J. Phys. Chem. C*, 2020, **124**(49), 26699–26713, DOI: 10.1021/acs.jpcc.0c09082.

32 G. F. Huttig and E. V. Schroeder, Hydrates of uranium tetroxide and trioxide, *Z. Anorg. Allg. Chem.*, 1922, **121**, 243.

33 J. Li, A. C. Maier and M. Jonsson, Stability of Studtite in Aqueous Suspension: Impact of HCO3– and Ionizing Radiation on the Dynamics of Dissolution, *ACS Appl. Energy Mater.*, 2020, **3**(1), 352–357, DOI: 10.1021/acsaem.9b01611.

34 D. K. Unruh, A. Burtner, L. Pressprich, G. E. Sigmon and P. C. Burns, Uranyl peroxide closed clusters containing topological squares, *Dalton Trans.*, 2010, **39**(25), 5807–5813, DOI: 10.1039/C0DT00074D.

35 P. C. Burns, K.-A. Kubatko, G. Sigmon, B. J. Fryer, J. E. Gagnon, M. R. Antonio and L. Soderholm, Actinyl Peroxide Nanospheres, *Angew. Chem., Int. Ed.*, 2005, **44**(14), 2135–2139, DOI: 10.1002/anie.200462445.

36 K. Walenta, On studtite and its composition, *Am. Mineral.*, 1974, **59**(1–2), 166–171.

37 M. A. Rodriguez, P. E. Weck, J. D. Sugar and T. J. Kulp, Powder X-ray diffraction of Metastudtite, $(UO_2)O_2(H_2O)_2$, *Powder Diffr.*, 2016, **31**(1), 71–72, DOI: 10.1017/S0885715615000895, From Cambridge University Press Cambridge Core.

38 L. J. Augustine, H. Rajapaksha, M. M. F. Pyrch, M. Kasperski, T. Z. Forbes and S. E. Mason, Periodic Density Functional Theory Calculations of Uranyl Tetrachloride Compounds Engaged in Uranyl–Cation and Uranyl–Hydrogen Interactions: Electronic Structure, Vibrational, and Thermodynamic Analyses, *Inorg. Chem.*, 2023, **62**(1), 372–380, DOI: 10.1021/acs.inorgchem.2c03476.

39 (*a*) CCDC 2528711: Experimental Crystal Structure Determination, 2026, DOI: 10.25505/fiz.icsd.cc2qwbb9; (*b*) CCDC 2528712: Experimental Crystal Structure Determination, 2026, DOI: 10.25505/fiz.icsd.cc2qwbcb.